Modeling of depressurization-induced superheating for compressed liquefied gases

Wentian Zheng[†], *Haroun Mahgerefteh,**[†], *Didier Jamois*[‡], *Jerome Hebrard*[‡], *Christophe Proust*[‡]

[†] Department of Chemical Engineering, University College London, London WC1E 7JE, U.K.

[‡] INERIS, Parc Technologique ALATA, Verneuil-en-Halatte BP 2 60550, France

During the rapid depressurization of a liquefied gas, its superheating may lead to a Boiling Liquid Expanding Vapor Explosion (BLEVE). Such risk is of enormous concern during Carbon Capture and Storage (CCS) given the significant amounts of pressurized CO_2 involved during its transportation and storage. This paper for the first time presents the development and validation of a rigorous split-fluid blowdown model for predicting the degree of superheat following the rapid decompression of liquefied gases or two-phase mixtures with particular reference to CO_2. The model is successfully validated based on the comparison of the predicted vapor and liquid phase pressures and temperatures against the recorded data from a number of depressurization tests conducted for pure dense-phase CO_2 and its mixtures representing those associated with the different capture technologies. The impacts of the changes in the pressure relief valve diameter and the CO_2 purity on the degree of superheat and hence the spontaneity in undergoing a BLEVE is investigated using the model.

Keywords: CO_2, CCS, BLEVE, transportation safety, superheating, vessel blowdown

1. INTRODUCTION

Boiling Liquid Expanding Vapor Explosion (BLEVE) is defined as an explosion resulting from rupture of high pressure liquefied gases containments[1]. The formed blast waves, flying fragments and further release of toxic contents can cause serious damage to property, people and the environment. For hydrocarbons such as Liquefied Natural Gas (LNG), a BLEVE is mostly caused by the containment subjected to external fire attack[2]; the released gaseous fuel effectively mixes with ambient air and a chemical explosion takes place upon ignition. Given its relatively high frequency of occurrence, hydrocarbon BLEVEs are routinely considered as a credible failure scenario during the risk assessment in the process engineering industry.

On the other hand, although less frequent, for some pressurized non-flammable liquefied gases, a BLEVE can still occur due to the superheating of the liquid phase following its rapid depressurization during emergency blowdowns or in the event of accidental containment failures (e.g. vessel ruptures). Superheating occurs when there is a delay, often referred to as thermal relaxation[3], for the vapor to evolve from the liquid phase upon a rapid drop in the pressure thereby attaining a temperature which is higher than its saturated value. The difference between these two temperatures is termed as the degree of superheat. The higher its value, the larger is the risk of a BLEVE.

To date, the few reported BLEVE incidents involving non-flammable fluids have been primarily confined to CO_2. For example, a BLEVE following the accidental puncture of a fire extinguisher containing only 5 kg of liquid CO_2 in Norway resulted in the extinguisher debris being projected more than 35 m[4].

A far more catastrophic incident involving a CO_2 BLEVE occurred in Worms, Germany in 1994[5]. Here, the blast wave and flying fragments following the puncture and BLEVE of a liquefied CO_2 storage tank resulted in three fatalities and significant property damages.

Given the emergence of Carbon Capture and Storage (CCS) as a key technology for mitigating the impact of global warming, with safety being a headline issue[6], assessing the risk of a BLEVE during such operations is critically important. This is in view of the significant amounts (hundreds to thousands of tons) of pressurized CO_2 involved during its pipeline transportation and intermediate storage. Here, rapid depressurization can occur either intentionally, during for example, maintenance or emergency blowdown, or accidentally following containment failure. Additionally, considering the fact that the most economical way for the pipeline transportation of CO_2 for subsequent storage is in its dense or supercritical state[7], and that CO_2 at concentration greater than 7 v/v% is an asphyxiant[8] underlines the importance of considering a BLEVE as a key feature for CCS risk assessment. To date, there is little evidence for the above having been accounted for.

A simplistic method for determining the risk of a BLEVE occurring is based on the 'Superheat Limit Temperature' (SLT) theory[9–11]. Here, SLT can be computed from an equation of state (EoS) from solving $\left(\partial p/\partial \rho\right)_T = 0$ (i.e. the spinodal curve). However, in the investigation of the accuracy of modern EoS in predicting the metastable states of fluids, Aursand et al.[12] showed a noticeable deviation of the predicted SLT by the EoS considered from available experimental data. Alternatively, the Classical Nucleation Theory (CNT) based on the modeling of bubble dynamics was observed to produce an improved accuracy. A BLEVE is then said to occur if the resulting liquid phase temperature exceeds the SLT.

However, based on lab scale tests[4], Bjerketvedt et al. reported the occurrence of CO_2 BLEVEs at liquid temperatures lower than the SLT. The same conclusion was also reached by Prugh[13] in his study of the hazards associated with BLEVEs, where the intensity of a BLEVE was related to the degree of superheat during depressurization.

In view of the above, the development of a rigorous mathematical model for predicting the induced superheating during the rapid depressurization of liquefied gases is pivotal.

BLOWDOWN developed by Haque et al.[14,15] is the earliest and arguably the most relevant depressurization model developed for condensable hydrocarbon mixtures. BLOWDOWN accounts for heat transfer interphase mass transfer and thermal stratification (*i.e.* temperature differences) between the constituent fluid zones. The latter includes the vapor, liquid and any free water. An Equation of State (EoS) based on the extended principle of corresponding states[16] is employed to provide the pertinent vapor/liquid phase equilibrium data. However, the prediction of the interphase mass transfer between the constituent liquid and vapor phases is based only on the mass fractions and settling velocity of the evolved liquid droplets. No superheating of the liquid phase is accounted for.

More recently, D'Alessandro et al.[17] employed the concept of partial phase equilibrium, first introduced by Speranza and Terenzi[18] in their blowdown model. Here, the condensed liquid and the evaporated vapor are assumed to be at thermal equilibrium with their respective original bulk phases. The authors refer to the original bulk phases and the formed bubble or liquid droplets as the parent and child phases respectively. The latter are further assumed to mix with the opposite parent phases instantaneously. As such, the interphase mass transfer between the liquid and vapor zones is purely determined based on equilibrium flash calculations thereby ignoring any superheating of the liquid phase.

The thermal equilibrium assumption has been widely adopted in high-pressure CO_2 pipeline decompression modeling[19–23]. Featured examples include the multi-phase and multi-component flow model by Mahgerefteh et al.[19] and the vapor-liquid-solid three-phase CO_2 mixture decompression model by Martynov et al.[20]. However, in spite of their sophistication in

accounting for important fluid flow phenomena such as decompression wave propagation and wall friction, the superheating of the liquid phase during rapid decompression has not been considered.

To account for such behavior, Deligiannis and Cleaver[24] incorporated an empirical non-equilibrium interphase mass transfer relation into their depressurization model. The ideal gas EoS was applied to the vapor phase and the model was validated against small-scale (0.2 m height, 0.034 m i.d cylindrical vessel) high pressure release experiments for refrigerant Freon 12 (R12) producing an over-estimate of the pressure trajectory. Additionally, the model's predictions were found to be sensitive to a number of empirical constants such as heterogeneous nucleation.

A more compact and computationally efficient non-equilibrium model based on a linear thermal relaxation relation accounting for the delay in bubble evolution from the liquid phase was proposed by Bilicki and Kestin[25] in their theoretical study of the impacts of the superheating of the liquid phase on wave propagation. The wave speed of a homogeneous two-phase system with superheated liquid phase was found to differ significantly from that of a system at thermal equilibrium.

Brown et al.[26] incorporated the same linear thermal relaxation relation proposed by Bilicki and Kestin[25] in their model to simulate outflow following the full-bore rupture of a real 144 m long, 0.15 m i.d pipeline containing liquid phase CO_2, obtaining relatively good predictions of the pipeline depressurization trajectory. However, their model is based on the assumption of fully dispersed flow during depressurization, found to be valid for pipeline full-bore rupture failures only. In the event of fluid phase separation (often encountered during vessel blowdown of

multiphase mixtures), heterogeneous behavior such as thermal stratification between the vapor and liquid phases invalidates the imposed assumption.

This paper presents the development and validation of a multi-component split fluid depressurization model accounting for the superheating of the liquid phase. The depressurization of pure CO_2 and its mixtures are chosen as the test cases to validate the model, given their significant relevance to CCS. The work proceeds as follows. Section 2 gives a description of the model development including the modeling of the superheating of the liquid phase and its extension to multi-component mixtures. The numerical solution method for solving the resulting set of ordinary differential equations for the blowdown model is presented in Section 3. In Section 4, the model developed is validated against data recorded from a series of high pressure release experiments for pure CO_2 and its mixtures. In addition, case studies investigating the impact of relaxation time, orifice diameter and the type of CO_2 impurities on the degree of superheat are conducted and the results are discussed. Conclusions and suggestions for further work are presented in Section 5.

2. THEORY

2.1 Thermodynamics. For predictions of fluid thermal properties spanning its supercritical, liquid (including superheated liquid (metastable liquid)), vapor-liquid and vapor states, GERG-2004 EoS built in the commercial thermodynamic package, REFPROP[27] is employed in this study.

For fluids at equilibrium, in comparison with a cubic EoS such as the Soave-Redlich-Kwong (SRK)[28] and Peng-Robinson (PR) EoS[29], the GERG-2004 EoS is superior especially in supercritical or near-critical regions. According to Valderrama[30], cubic EoS with mixing rules usually produce a typical deviation of ± 10% from experimental measurements for various multi-component mixtures in supercritical regions. In contrast, multi-component Helmholtz energy

EoS (e.g. GERG-2004 EoS) with appropriate mixing rules gives accurate predictions over the entire thermodynamic space[31].

With regards to the non-equilibrium predictions, according to the investigation of the accuracy of modern equation of state (EoS) on the predictions of metastable states of single- and multi-component fluids by Aursand et al.[12], the uncertainty in an EOS is characterized by the deviation of the predicted superheating limit temperatures (SLT) from experimental measurements. For superheated (metastable) liquids, this is reported between 1.4 and 2.7 K using multi-parameter EoS (e.g. GERG-2004 EoS[31]) which is similar to the other EoS investigated (including cubic[29] and PC-SAFT EoS[32]).

2.2 Blowdown model formulation. Figure 1 is a schematic representation of a vessel during blowdown showing the vapor zone, *G* and liquid zone, *L*. The pertinent fluid properties along with their definitions are given in the figure caption.

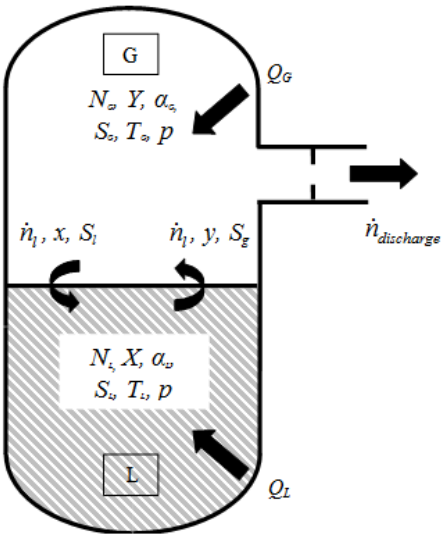

N = number of moles

Y = component mole fractions in the vapor zone, G

X = component mole fractions in the liquid zone, L

α = volume fractions of the fluid zones

S = specific entropy

T = temperature

P = pressure

$\dot{n}_g$ = mole rate of evaporation

$\dot{n}_l$ = mole rate of condensation

$\dot{n}_{discharge}$ = discharge mole flowrate

y = component mole fractions in the evaporated vapor, g

x = component mole fractions in condensed liquid, l

Q_G = heat exchange between the vapor zone, G and the dry vessel wall

Q_L = heat exchange between the liquid zone, L and the wet vessel wall

Figure 1: A schematic representation of a pressure vessel during rapid depressurization showing the pertinent parameters for blowdown modeling.

2.2.1 Vapor zone. During depressurization, the vapor zone and any resulting condensed liquid formed are assumed to be in equilibrium. Accordingly, the corresponding number of moles of the condensed liquid is simply obtained from an equilibrium flash calculation. It is also assumed that the condensed liquid immediately and homogeneously mixes with the liquid zone below it.

The mole balance for the vapor zone is given by:

$$\frac{d\rho_G \alpha_G}{dt} = \frac{1}{V_T}\left(\dot{n}_g - \dot{n}_l - \delta \dot{n}_{discharge}\right) \tag{1}$$

where V_T is the total volume of the containment. For a vessel or short pipeline, it is obtained by assuming a perfect cylindrical shape. Depending on the fluid zone upstream of the discharge orifice, δ takes the value of 0 (liquid zone) or 1 (vapor zone). The rest of the symbols are defined in Figure 1.

The energy conservation for the vapor zone based on the second law of thermodynamics with the assumption of infinitesimal heat transfer[33] is given by:

$$\frac{d\rho_G \alpha_G S_G}{dt} = \frac{1}{V_T}\left(\dot{n}_g S_g - \dot{n}_l S_l - \delta\dot{n}_{discharge} S_{discharge} + \frac{\dot{Q}_G}{T_G} \right) \tag{2}$$

where $S_{discharge}$ is the specific entropy of the discharging fluid from the vessel, and is equal to either S_G or S_L depending on which fluid zone is subjected to discharge.

For the heat transfer from the vessel wall to the vapor zone, natural convection is the dominating heat transfer mode[14,34] and the overall heat transfer coefficient, U_G is determined based on Churchill and Chu's correlation for natural convection[35]:

$$Nu_G = \left(0.835 + \frac{0.387 Ra_G^{1/6}}{\left(1 + \left(0.492/Pr_G\right)^{9/16}\right)^{8/27}} \right) \tag{3}$$

where the vapor zone Nusselt number, Nu_G, Rayleigh number, Ra_G and Prandtl number, Pr_G are respectively defined as:

$$Nu_G = \frac{U_G D_H}{k_G} \tag{4}$$

$$Ra_G = \frac{D_H^3 \rho_G^2 g \beta_G \left(T_{GW} - T_G\right)}{\mu_G^2} Pr_G \tag{5}$$

$$Pr_G = \frac{Cp_G \mu_G}{k_G} \tag{6}$$

where D_H is the characteristic length taken as the diameter of the containment considered. β_G is the isothermal expansion coefficient, $-\left(\partial\rho/\partial T\right)_p/\rho_G$. The thermal conductivity, k_G, viscosity, μ_G and heat capacity, Cp_G are evaluated at film temperature defined as $\left(T_G + T_{GW}\right)/2$ using REFPROP[27].

The temperature gradient within the vessel wall is neglected given steel's high thermal conductivity (*ca.* 40 w/m·K[36]). The heat transfer rate, $\dot{Q}_G$ is then given by:

$$\dot{Q}_G = U_G A_G \left(T_{GW} - T_G\right) \tag{7}$$

where A_G and T_{GW} are respectively the dry wall heat transfer area and its temperature. For interface heat transfer, that associated with mass transfer is dominant (first two terms in the parentheses of equation 2), and the thermal conduction is thus neglected[14,33].

2.2.2 Liquid zone. The modeling of the liquid zone is analogous to that of the vapor, with the exception of the consideration of the possible superheating. Given that vaporization stops upon reaching thermal equilibrium, a relaxation equation based on the linear approximation proposed by Bilicki and Kestin[25] is employed to account for the delay in vaporization. This is given by:

$$\frac{dq}{dt} = -\frac{q - q_{eq}}{\tau} \tag{8}$$

where q is the mole fraction of the evaporated vapor from the liquid zone, q_{eq} is the corresponding equilibrium vapor mole fraction, and τ is the relaxation time governing the rate at which the system approaches its thermal equilibrium state.

By neglecting the bulk fluid motions within the confinement, integrating Equation 8 over the depressurization time step, *i-1* to *i* produces:

$$q_i = q_{eq,i} - \left(q_{eq,i} - q_{i-1}\right) exp\left(-\frac{t}{\tau}\right) \tag{9}$$

A closure relation is required to calculate the characteristic relaxation time, τ in Equation 9. In the absence of such data for CO_2 and its mixtures, constant relaxation times are used in all simulations, which were determined to produce the best agreement between the theoretical predictions and measured data in all cases.

The corresponding numbers of moles of the evolving vapor can then be easily calculated based on the relation:

$$n_g = N_L q_i \tag{10}$$

The evaporated vapor from the liquid zone is assumed to be in saturated state at the system pressure, whilst the remaining liquid phase may be in superheated state.

Figure 2 shows the calculation flow diagram for determining the fluid thermal states of the evaporated vapor and the superheated liquid for both single- and multi-component systems. The iterative solutions of T_L and α_L are updated using a Newton-Raphson type method implemented in DNSQE non-linear solver[34]. The extension of the superheating model presented above to multi-component mixtures is achieved by performing the additional component mole balances.

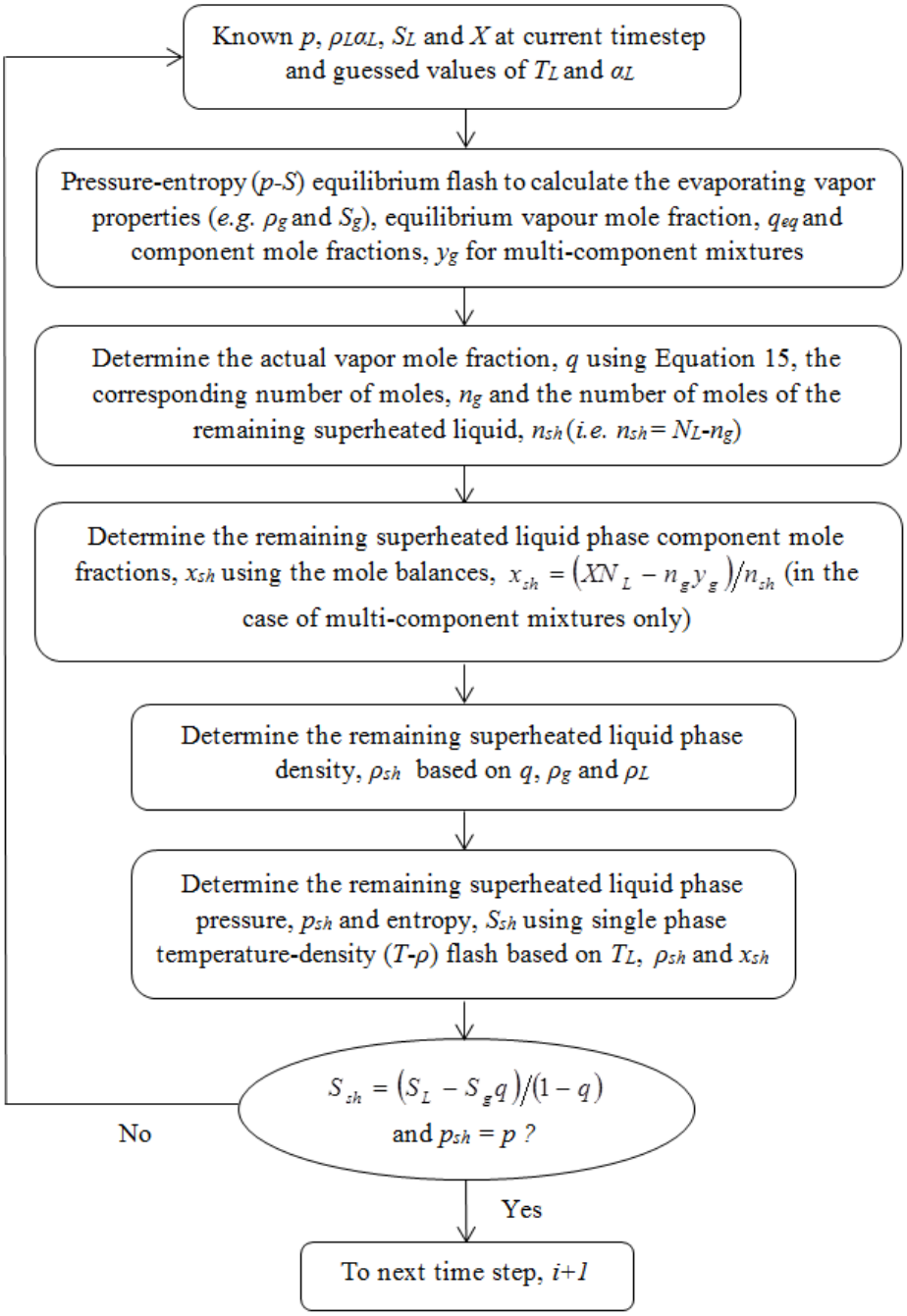

Figure 2. The calculation flow diagram for determining the thermal states of the superheated liquid phase and the evaporated vapor.

Finally, the resulting mole and energy balances for the liquid zone are respectively presented below:

$$\frac{d\rho_L \alpha_L}{dt} = \frac{1}{V_T}\left(\dot{n}_l - \dot{n}_g - \delta\dot{n}_{discharge}\right) \tag{11}$$

$$\frac{d\rho_L \alpha_L S_L}{dt} = \frac{1}{V_T}\left(\dot{n}_l S_l - \dot{n}_g S_g - \delta\dot{n}_{discharge} S_{discharge} + \frac{\dot{Q}_L}{T_L}\right) \tag{12}$$

Boiling is assumed to be the main heat transfer mode in the liquid zone. The corresponding heat transfer rate, $\dot{Q}_L$ is estimated based on Rohsenow's correlation[35] given by:

$$\dot{Q}_L = \mu_L h_{fg}\left(\frac{g\left(\rho_L - \rho_g\right)}{\sigma}\right)\left(\frac{Cp_L\left(T_{LW} - T_L\right)}{0.013 h_{fg} Pr_L^1}\right)^3 \tag{13}$$

where μ_L, σ, h_{fg} and Cp_L are respectively the viscosity, the surface tension, the latent heat and the constant pressure heat capacity of the liquid zone computed by REFPROP[27]. For a multi-component mixture, the latent heat is calculated from the enthalpy difference of its dew point and bubble point at a given pressure. T_{LW} is the wet wall temperature and Pr_L is the liquid zone Prandtl number.

2.3 Discharge modeling. Three different methods are employed to simulate the choked flow through the discharge orifice depending on the fluid phase. These include the Blevins' model in the case of pure vapor phase discharge, the maximization of the mole flowrate method for two-phase discharge and the Bernoulli's equation for liquid phase discharge. The corresponding formulations are given below.

2.3.1 Vapor phase discharge[38]. The vapor phase discharge mole flowrate is given by:

$$\dot{n}_{discharge} = \begin{cases} C_d A_{orifice} \sqrt{r\rho p} \left(\frac{2}{r+1} \right)^{r+1/2(r-1)}, \\ \frac{p_{amb}}{p} \geq \left(\frac{2}{r+1} \right)^{r/(r-1)}; \\ C_d A_{orifice} \left(\frac{p_{amb}}{p} \right)^{1/r} \sqrt{\frac{2r}{r-1} p\rho \left(1 - r^{r-1/r}\right)}, \\ \frac{p_{amb}}{p} < \left(\frac{2}{r+1} \right)^{r/(r-1)} \end{cases} \quad (14)$$

where, p, T, ρ and r are respectively the pressure, the temperature, density and isentropic expansion coefficient of the vapor zone. p_{amb}, $A_{orifice}$ and C_d on the other hand denote the ambient pressure, the discharge orifice area and the discharge coefficient respectively.

The isentropic expansion coefficient is determined by:

$$r = \frac{\rho}{p} \frac{Cp}{Cv} \left(\frac{\partial p}{\partial \rho} \right)_T \quad (15)$$

2.3.2 Two-phase discharge[39]. The conditions for two-phase choked flow can be determined through maximizing the discharge flowrate by varying the orifice pressure, $p_{orifice}$ isentropically. The discharge mole flowrate in terms of the predicted choked conditions at the orifice is given by:

$$\dot{n}_{discharge} = \rho_{orifice} C_d A_{orifice} \left(2\left(h - h_{orifice}\right)\right)^{1/2} \quad (16)$$

where h is the known specific enthalpies of the vapor or liquid zone, and $h_{orifice}$ is determined by a pressure-entropy *(p-S)* flash calculation at $p_{orifice}$ and $S_{orifice}$.

2.3.3 Liquid phase discharge. Following Richardson et al.[40] for non-flashing incompressible liquid discharge, the Bernoulli's equation can be applied to determine the mass flow rate:

$$p + \frac{\rho u^2}{2} = p_{orifice} + \frac{\rho u_{orifice}^2}{2} \quad (17)$$

where u is the flow velocity in the vessel which is often negligible (stagnant conditions). Given that $p_{orifice}$ is equal to the ambient pressure, $u_{orifice}$ and hence the discharge flow rate can be calculated by rearranging Equation 17.

3. NUMERICAL SOLUTION METHOD

The blowdown model presented above consists of a system of Ordinary Differential Equations (ODE) which may be written in the following vector form:

$$\frac{d\boldsymbol{U}}{dt} + \boldsymbol{F}(\boldsymbol{U}) = \psi \tag{18}$$

where,

$$\boldsymbol{U} = \begin{bmatrix} \rho_G \alpha_G \\ \rho_L \alpha_L \\ \rho_G \alpha_G S_G \\ \rho_L \alpha_L S_L \end{bmatrix}, \qquad \boldsymbol{F(U)} = \begin{bmatrix} \dot{n}_{outflow}\delta \\ \dot{n}_{outflow}\delta \\ \dot{n}_{outflow} S_G \delta - \dfrac{\dot{Q}_G}{T_G} \\ \dot{n}_{outflow} S_L \delta - \dfrac{\dot{Q}_L}{T_L} \end{bmatrix} \tag{19}$$

are respectively referred as the vector of conservative variables and their functions. $\boldsymbol{\psi}$**,** is the vector containing the source terms which corresponds to the interphase mass transfer and the associated entropy exchange:

$$\psi = \begin{bmatrix} \dot{n}_g - \dot{n}_l \\ \dot{n}_l - \dot{n}_g \\ \dot{n}_g S_g - \dot{n}_l S_g \\ \dot{n}_l S_l - \dot{n}_g S_g \end{bmatrix} \tag{20}$$

The solution strategy for above ODE system is analogous to that adopted in the study by D'Alessandro et al.[17]. At each time step, the ODE system is solved firstly without taking the source terms into account. Thereafter, the contributions of the source terms are added to update

the conservative variables explicitly within the same time step. Finally, the fluid thermal states of each fluid zone are updated to allow the solution to advance in time.

4. RESULTS AND DISSCUSSIONS

The following presents the validation of the depressurization model described above by comparison of its predictions against the published data obtained from two sets of depressurization experiments; one for pure CO_2 conducted by TNO and DNV[41], the other for CO_2 with impurities conducted by INERIS as part of the CO2PipeHaz project[42].

4.1 ***DNV and TNO high pressure vessel release experiments.*** In the DNV and TNO high pressure vessel release experiments[41], a horizontal 610 mm o.d, 30 mm wall thickness and 2000 mm height cylindrical stainless steel vessel was connected to nozzles of different discharge orifice diameters including 3, 6 and 12 mm at its bottom. The vessel was instrumented with two thermocouples (Cu-Ni type with ± 1 K accuracy) located at its top and bottom to measure the fluid temperatures. A pressure transmitter (± 0.3% accuracy, 0.001 s response time) located at the top of the vessel recorded the system pressure.

For all three releases performed, the test vessel was initially completely filled with pure CO_2 at the pressure and temperature ranges of 115 to 120 bar and of 296 to 300 K corresponding to the liquid phase. Table 1 gives the various temperatures, pressures and the time lapsed following the onset of depressurization to reach the fluid saturated conditions for each test. The latter corresponds to the time at which the recorded temperature-pressure depressurization path crosses the CO_2 saturation curve.

It is noted that all the three depressurization tests (see Table 1) were started prior to the thermal equilibration between the vessel top and bottom temperatures. The authors attributed this temperature difference to the filling process.

The simulations were performed using 0.001 s time step. Convergence test shows that further decreasing the time step to as low as 0.0001 s had a marginal impact on the simulated data. The relaxation time, τ was set to be 0.5 s. For the sake of comparison, the same runs are repeated using BLOWSIM[33], validated against the commercially available blowdown computer program, BLOWDOWN[14].

Figures 3a-c show the comparisons of the pressure predictions against the recorded experimental data for the three orifice diameters during depressurization.

Returning to Figures 3a-c, as it may be observed good agreement between the present model and experiment for all three releases is obtained. BLOWSIM on the other hand consistently under-predicts the rate of depressurization

The data show two distinctive trends: an initial rapid drop in pressure where the fluid remains in the liquid phase; this is soon followed by a much slower depressurization rate corresponding to the onset of the fluid phase transition into the two-phase region as marked by the dashed vertical line. Also, as expected the depressurization rate markedly increases with an increase in the orifice diameter (as reflected in the shorter initial period of rapid pressure drop marked by the dashed line). Time lapsed to reach 40 bar pressure for 3, 6, 12 mm orifice diameters are 1200, 300, 30 s respectively.

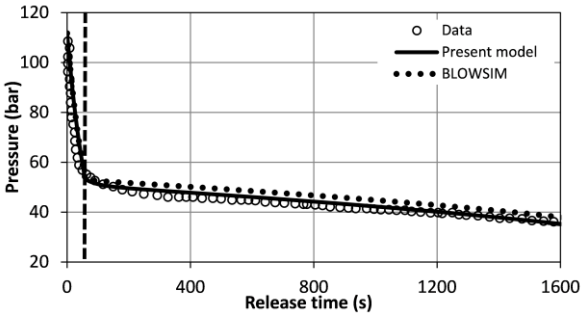

(a)

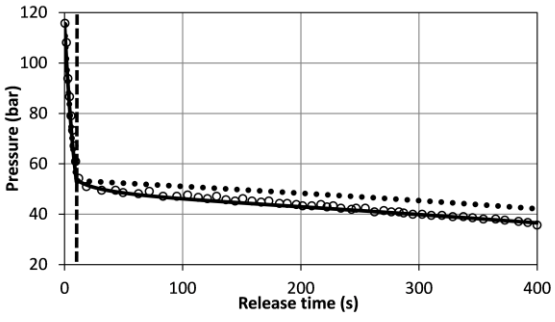

(b)

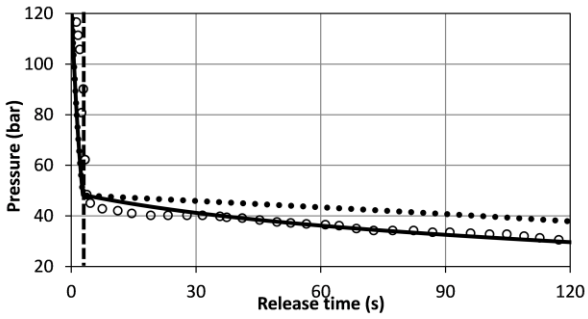

(c)

Figure 3: Variation of the pressure with time for different discharge orifice diameters of 3 mm (a), 6 mm (b) and 12 mm (c).

Figures 4a-c represent the corresponding comparison for the vapor (top) and liquid (bottom) zone temperatures during depressurization for the different orifice diameters. The equilibrium temperatures corresponding to the measured pressures are also included to showcase the experimentally observed superheating in the liquid zone.

As it may be observed, in all cases, the vapor zone temperature stays relatively constant over the entire depressurization period, dropping by a maximum value of 5 K. The drop in the liquid zone temperature is however more significant than that in the vapor zone. The lower observed drop in the vapor zone temperature can be mainly attributed to the lower heat capacity and molar density of the vapor as compared to the liquid along with the latent heat effect which cools the liquid undergoing evaporation.

It is noteworthy that in the case of the liquid zone data, the model predictions accounting for superheating again demonstrate better agreement with the recorded data as compared to BLOWSIM. At any given time, the BLOWSIM prediction of liquid zone temperature is consistently lower than the corresponding measured value.

Taking the difference between the measured liquid zone temperatures and the equilibrium temperatures at the measured pressures gives the degree of superheat. It is observed to increase

(up to ca. 15 K) with a larger release orifice diameter, which indicates an increase in the risk of a BLEVE.

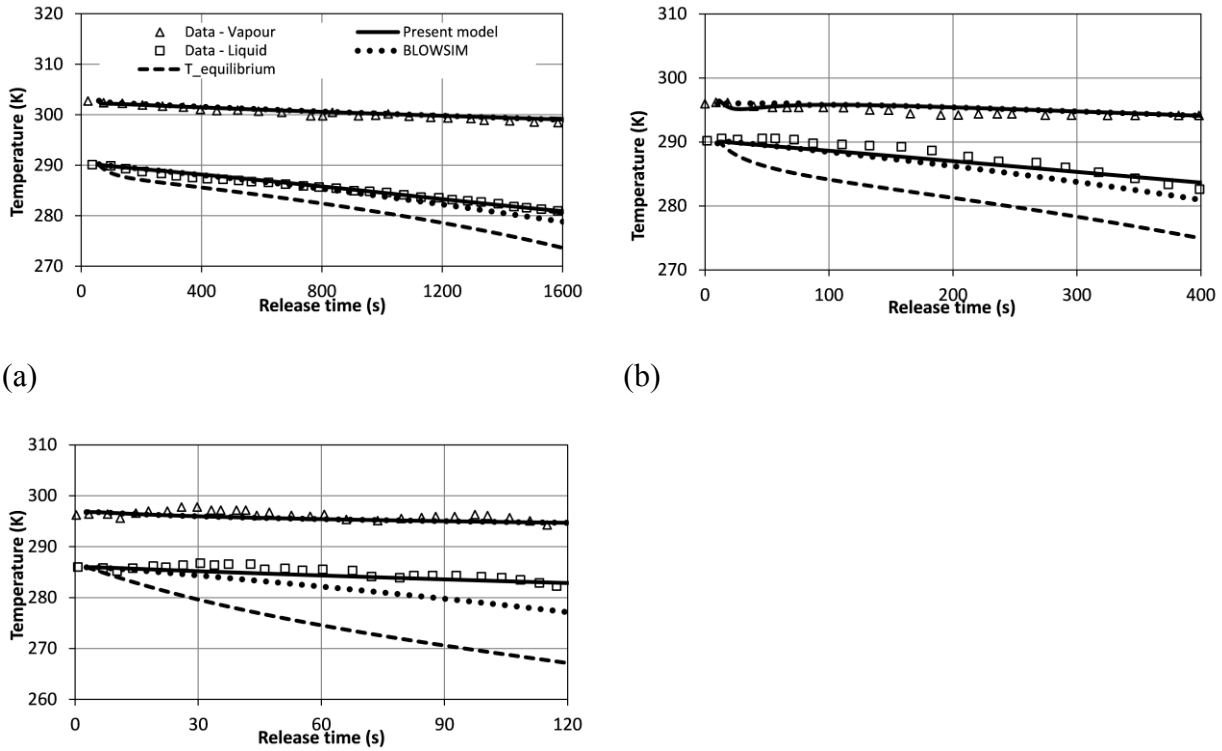

(a) (b)

(c)

Figure 4. Variations of liquid and the vapor zone temperatures with time for different discharge orifice diameters of 3 mm (a), 6 mm (b) and 12 mm (c).

Such a trend is elucidated by plotting the corresponding depressurization paths in pressure-temperature (*p*-*T*) plane together with the SLT curve for CO_2 (see Figure 5). As the valve diameter increases, the decompression path departs further from the saturation line. Nevertheless, these paths are still away from the SLT, and according to the SLT theory, no BLEVE would occur.

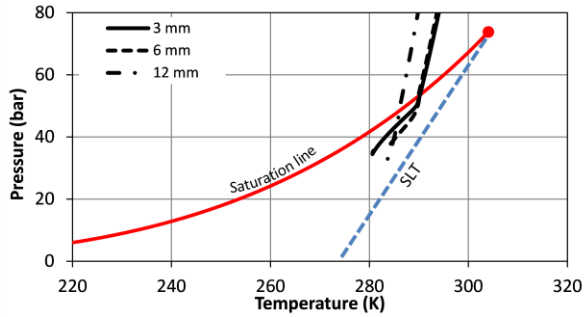

Figure 5: Predicted decompression paths for TNO & DNV tests in pressure-temperature (*p*-*T*) plane.

4.2 ***INERIS high pressure pipe release experiments*****.** As part of the course of our collaborative CO2PipeHaz European Commission project[42], a number of pipeline depressurization tests were conducted by the consortium partner, INERIS for pure CO_2 and its mixtures including CH_4 and N_2. Table 2 shows the conditions for the selected tests as examples for validation purposes in the present study.

The 37 m length, 50 mm i.d, 10 mm thickness stainless steel pipe incorporated various orifice diameter nozzles (4 mm, 6 mm and 12 mm) at one end and instrumented with 4 fast response pressure transmitters (KISTLER type A4045 with ± 0.5 bar accuracy) evenly distributed along its length to measure the fluid pressure. At the same locations, temperature measurements were taken at the top, middle and bottom of the cross-section of the pipe using 12 thermocouples (6K type) protruding into the pipe.

Figures 6a-c and 7a-c show the simulated transient pressure and temperature (both at the top and the bottom of the containment) data for each test (see Table 2). A time step size of 0.001 s was used with a constant relaxation time of 0.01 s.

The corresponding recorded data are also presented for comparison. It should be noted that all the pressure and temperature transducers produced very similar measurements at the different locations along the pipe thus indicating a 'vessel-like' behavior where fast pressure equilibration

and negligible bulk fluid motions are expected along the pipe during depressurization. Although, for a longer pipeline (e.g. a few kilometers), pressure equilibration may not be as fast and the effect of wave propagation should be accounted for.

According to Figures 6a-c, good agreement between pressure predictions and the experimental data is obtained in all cases. Unlike the trend observed in the TNO & DNV tests, the pressure drop appears to be much more smooth and linear as the initial conditions of the containing fluid are very close to the phase boundary.

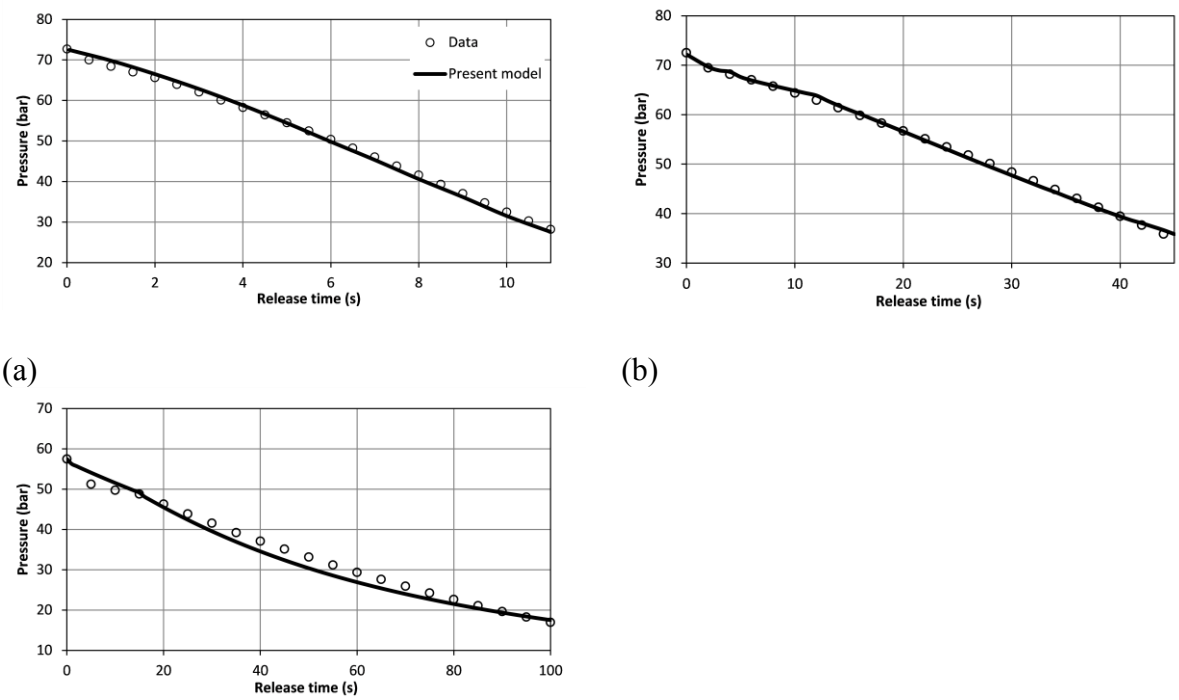

Figure 6. Variation of pressure with time during INERIS test 2 (a), 9 (b) and 16 (c).

Referring to the temperature data (Figures 7a-c), also included are the corresponding liquid phase saturated values based on assuming thermal equilibrium between the bulk liquid and the evolving vapor.

As it may be observed, much the same as the TNO & DNV tests presented earlier, the subsequent cooling in the liquid zone following depressurization is much more significant than that in the vapor zone, producing a maximum temperature drop of 30 K (see Figure 7c) .

More interestingly, soon after the depressurization commences, the simulated liquid zone temperature remains higher than the equilibrium values (dashed line), indicating the superheating of the liquid phase. The degree of the superheat increases with depressurization, reaching a maximum value of ca. 5 K (see Figure 7a).

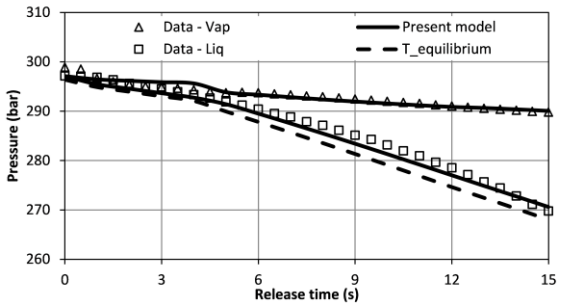

(a)

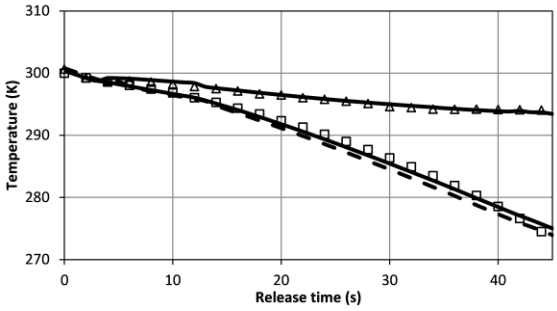

(b)

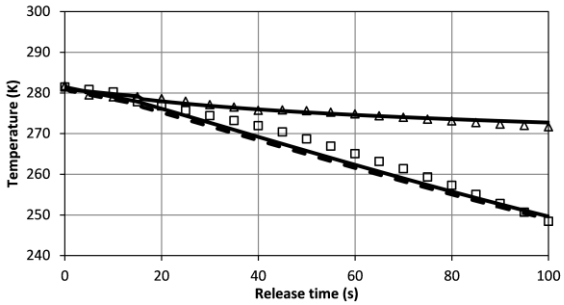

(c)

Figure 7: Variation of the liquid and vapor zone temperatures with time during INERIS test 2 (a), 9 (b) and 16 (c).

4.3 Impact of the relaxation time. According to equation 8, the relaxation time, τ reflects deviations of decompression fluids form thermodynamic equilibrium. To numerically illustrate its impact, simulations with different constant values of τ (covering the range of 0.005 to 0.5 s)

are performed adopting the exact setup from the simulation of INERIS test 16 (see Table 2). The predicted and measured transient pressure and temperature data are plotted in Figures 8a and b respectively; also included in Figure 8b is the equilibrium temperature (red curve) for references.

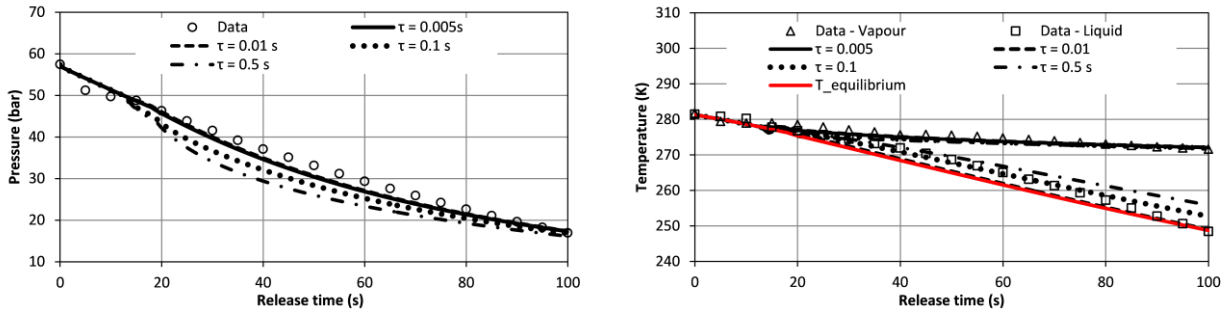

(a) (b)

Figure 8: Measured and predicted pressure (a) and temperature (b) variations with time applying different constant relaxation times (from 0.005 to 0.5 s).

In Figure 8a, a higher depressurization rate can be observed with an increase in the relaxation time. Turning to the temperature data (Figure 8b), for the liquid zone, higher degrees of superheat with larger τ are manifested in its predictions appearing further away from the equilibrium (red curve). With regards to the vapor zone, there is however no noticeable effect of τ.

4.4 Impacts of CO_2 purities and release diameters on the degree of superheat. The following presents the results of a series of simulations demonstrating the impacts of changing the release orifice diameters and the presence of impurities in CO_2 on the degree of superheat of the liquid phase during depressurization. For the sake of the analysis, the INERIS depressurization conditions corresponding to test 3 (see Table 2) are adopted.

To elucidate the impact of the release orifice diameter, simulations with three different orifice diameters of 6, 12 and 18 mm are performed with the same arbitrary mixture of 1.9 mol% N_2 and 98.1 mol% CO_2. The study of impact of impurities on the other hand is conducted by changing

N_2 impurity mole fractions from zero (pure CO_2) to 1.9 mol% whilst keeping the release orifice diameter at 18 mm. The time step and relaxation time are respectively set to 0.001 s and 0.01 s as previous. Other details for each of the 7 simulations with the assigned case study numbers are presented in Table 3.

Figures 9a-b shows the variation of the degrees of superheat with time during depressurization for all runs.

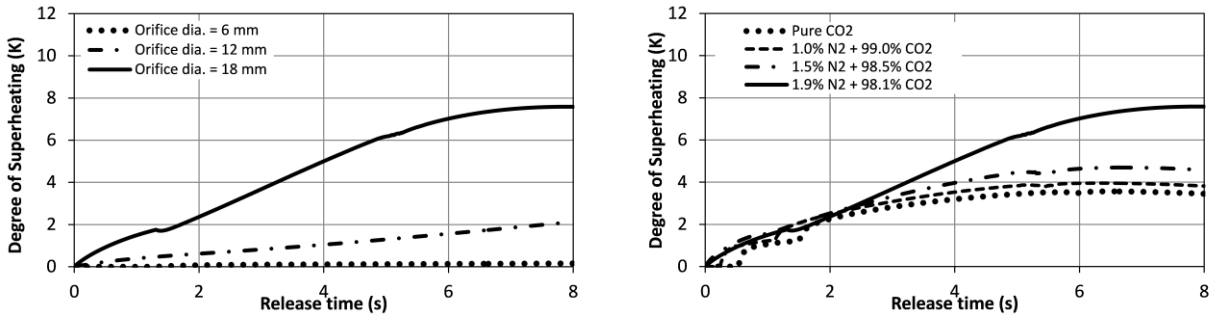

(a) (b)

Figure 9. Predicted variation of the degrees of superheat of the liquid phase with time in the orifice diameter (a) and CO_2 purity (b) case studies.

Referring to Figure 9a, as it may be observed, much the same as the TNO & DNV pure CO_2 vessel release tests findings, the degree of superheat of the liquid phase increases with the increase in the release orifice diameter; the maximum value reaching ca. 8 K for the 18 mm diameter orifice. This is believed to be a consequence of the higher depressurization rate due to the increase in orifice diameter. Accordingly, the delay in the vaporization becomes more significant and hence the observed higher degree of superheat in the liquid phase. The subsequent levelling off in the degree of superheat for the 18 mm diameter orifice after 6.5 s of depressurization is due to the drop of depressurization rate as the vessel evacuates.

The impact of impurities on superheating is shown in Figure 9b. In general, an increase in the mole fraction of N_2 impurity results in a monotonic increase in the degree of superheat,

indicating an increase in the risk of a BLEVE. The maximum difference of 4 K in the degree of superheat occurs between case studies 4 (pure CO_2) and 7 (with 1.9 mol% N_2 impurity).

5. CONCLUSIONS

This paper for the first time presented the development and validation of a multi-component split-fluid blowdown model for predicting the degree of superheat following the rapid depressurization of liquefied gases. Such modeling capability is of special relevance in the case of CCS given the significant amounts of CO_2 handled during its transportation, intermediate storage and geological sequestration. At any of these stages, rapid depressurization may occur following containment failure or during wanton blowdown for emergency or routine maintenance operations. Accordingly, although there is no recorded example of a CO_2 BLEVE occurring during controlled blowdown, such risk should not be ignored during CCS operations. Apart from the risk of a BLEVE resulting in potentially major destruction to property and fatalities, the migrating CO_2 cloud poses a significant hazard given that the gas is an asphyxiant at concentrations greater than 7 v/v %. This is the first time that such a potentially major hazard has been considered in detail in the context of CCS.

Model validation involved the comparison of its predictions against the recorded data from a number of high pressure experiments involving the release liquid phase CO_2 and its mixtures. Good agreement with the measurements of the temperatures and pressures for both of the separated vapor and the liquid zones, including the degree of superheat were obtained in all cases.

Additional case studies were performed using the validated model in order to elucidate the impacts of pressure relief diameter and CO_2 impurities on the degree of superheat. These investigations revealed that the degree of superheat and hence the risk of a BLEVE increases with an increase in the release orifice diameter. This is of special concern given the seemingly

logical inclination to depressurize units as fast as possible by increasing the relief diameter in an emergency situation.

In the case of CO_2 mixture investigations, it was found that the higher the mole fraction of the non-condensable component, the higher the degree of superheat and hence the greater the risk of a BLEVE occurring. This finding has significant implications given that depending on the capture technology employed, the captured CO_2 entering the high pressure transportation pipeline and ultimately the storage site will inevitably contain a range of impurities at different concentrations[43]. The impact of these impurities in the context of a BLEVE has never been considered prior to this work.

It is also worth noting that the model presented in this work is in principle applicable to blowdown under fire attack, provided that sufficiently small time discretization are employed for the numerical simulation such that heat transfer during each time step becomes negligible. However, this will be at a cost of prohibitive computational run times.

Finally, two important assumptions were made in the development of the model, both worthy of a future study. The first being no bulk fluid motion during depressurization. Although applicable in the case of high pressure storage vessels, in the case of pipelines, this assumption limits the application of the model to situations where normal flow in the pipeline has been terminated through emergency isolation prior to depressurization. The second, to do with the absence of relevant data or empirical correlations, is the use of a constant characteristic relaxation time to account for the delay in vaporization. Although despite the use of the constant relaxation time in this work, our model produces relatively good predictions within the ranges tested, the development of dedicated correlations for CO_2 and its mixtures at the relevant CCS operating pressures and temperatures should form the basis of a future study.

Table 1. Details of TNO & DNV high pressure vessel release experiments.

Release orifice diameter (mm)	Initial pressure (bar)	Initial top temperature (K)	Initial bottom temperature (K)	Average bulk fluid temperature (K)	Time to reach saturation following depressurization (s)
3	115	303	290	296.5	66
6	118	296	290	293.0	8
12	120	297	286	291.5	3

Table 2. Details of INERIS short pipeline release experiments.

Test No.	Orifice diameter (mm)	Initial pressure (bar)	Initial temperature (K)	Initial fluid phase	Mixture component mole fractions
3	12	72	300	Two-phase	1.9 mol% N_2 + 98.1 mol % CO_2
9	12	73	300	Liquid	1.6 mol% CH_4 + 98.4 mol% CO_2
16	6	57	281	Liquid	2.1 mol% CH_4 + 1.9 mol% N_2 + 96.0 mol% CO_2

Table 3: Details of INERIS short pipeline release simulations for investigating the impacts of discharge orifice diameters and CO_2 impurities on the degree of superheat.

Case study No.	Orifice diameter (mm)	Initial pressure (bar)	Initial temperature (K)	Initial fluid phase	Impurity mole fractions
Impact of the pressure relief valve diameters					
1	6	72	300	Liquid	1.9 mol% N_2
2	12				
3	18				
Impact of CO_2 purities					
4	18	72	300	Liquid	Pure CO_2
5					1.0 mol% N_2
6					1.5 mol% N_2
7					1.9 mol% N_2

ACKNOWLEDGEMENTS

The financial support from the European Union 7th Framework Programme FP7-ENERGY-2012-1-2STAGE under grant agreement number 309102 (CO2QUEST), the UK Engineering and Physical Science Research Council (UKCCSRC grant number UKCCSRC-C2-183) and from UCL Graduate School is gratefully acknowledged.

AUTHOR INFORMATION

Corresponding Author

*E-mail: h.mahgerefteh@ucl.ac.uk.

ABBREVIATIONS

CCS, Carbon Capture and Sequestration; PR-EoS, Peng-Robinson Equation of State; SRK-EoS, Soave-Redlich-Kwong Equation of State; ODE, Ordinary Differential Equation.

REFERENCES

(1) Englund, S. M.; Bodurtha, F. T.; Britton, L. G.; Crowl, B. A.; Grossel, S.; High, W. G.; Kletz, T. A.; Ormsby, R. W.; Owens, J. E.; Schiappa, C. A.; Siwek, R.; White, R. E.; Winegardner, D.; Woodward, J. *Perry's Chemical Engineers' Handbook*, 7th ed.; Perry, R. H., Green, D. W., Maloney, J. O., Eds.; McGraw-Hill: New York, 2008.

(2) McDevitt, C. A.; Chan, C. K.; Steward, F. R.; Tennankore, K. N. Initiation Step of Boiling Liquid Expanding Vapour Explosions. *J. Hazard. Mater.* **1990**, *25*, 169.

(3) Downar-Zapolski, P.; Bilicki, Z. The Non-Equilibrium Relaxation Model for One-Dimensional Flashing Liquid Flow. *Int. J. Multiph. Flow* **1996**, *22*, 473.

(4) Bjerketvedt, D.; Egeberg, K.; Ke, W.; Gaathaug, a.; Vaagsaether, K.; Nilsen, S. H. Boiling Liquid Expanding Vapour Explosion in CO_2 Small Scale Experiments. *Energy Procedia* **2011**, *4*, 2285.

(5) Clayton, W. E.; Griffin, M. L. Catastrophic Failure of a Liquid Carbon Dioxide Storage Vessel. *Process Saf. Prog.* **1994**, *13*, 202.

(6) Ritchie, A.; Green, C.; Harridge, D.; Chalmers, H.; Gibbins, J.; Tait, L.; Lavric, L.; Chapbell, M.; Sorensen, M.; Pountney, P.; Waite, P. *Carbon Capture and Storage Readiness*; Rio House: Bristol, 2008.

(7) Patchigolla, K.; Oakey, J. E. Design Overview of High Pressure Dense Phase CO_2 Pipeline Transport in Flow Mode. *Energy Procedia* **2013**, *37*, 3123.

(8) Harper, P.; Wilday, J.; Bilio, M. Assessment of the major hazard potential of carbon dioxide (CO_2) http://www.hse.gov.uk/carboncapture/assets/docs/major-hazard-potential-carbon-dioxide.pdf (accessed Dec 20, 2016).

(9) Reid, R. C. Superheated Liquids. *Am. Sci.* **1976**, *64*, 146.

(10) Skripov, V. P. *Metastable Liquids*; John Wiley & Sons, Inc.: New York, 1974.

(11) Skripov, V. P.; Sinitsyn, E. N.; Pavlov, P. A.; Ermakov, G. V.; Muratov, G. N.; Bulanov, N. V. *Thermophysical Properties of Liquids in the Metastale (superheated) State*; Gordon and Breach Science Publishers: New York, 1988.

(12) Aursand, P.; Gjennestad, M. A.; Aursand, E.; Hammer, M.; Wilhelmsen, Ø. The Spinodal of Single- and Multi-Component Fluids and Its Role in the Development of Modern Equations of State. *Fluid Phase Equilib.* **2017**, *436*, 98.

(13) Prugh, R. W. Quantify BLEVE Hazards. *Chem. Eng. Prog.* **1991**, *87*, 67.

(14) Haque, M. A.; Richardson, S. M.; Saville, G. Blowdown of Pressure Vessels Part I. Computer Model. *Trans IChemE* **1992**, *70*, 3.

(15) Haque, M. A.; Richardson, S. M.; Saville, G. Blowdown of Pressure Vessels. II. Experimental Validation of Computer Model and Case Studies. *Trans IChemE* **1992**, *70*, 1.

(16) Rowlinson, J. S.; Watson, I. D. The Prediction of the Thermodynamic Properties of Fluids and Fluid Mixtures, I. the Principle of Corresponding States and Tis Extensions. *Chem. Eng. Sci.* **1969**, *24*, 1565.

(17) D'Alessandro, V.; Giacchetta, G.; Leporini, M.; Marchetti, B.; Terenzi, A. Modelling Blowdown of Pressure Vessels Containing Two-Phase Hydrocarbons Mixtures with the Partial Phase Equilibrium Approach. *Chem. Eng. Sci.* **2015**, *126*, 719.

(18) Speranza, A.; Terenzi, A. Blowdown of Hydrocarbons Pressure Vessel with Partial Phase Separation. In *Applied and Industrial Mathematics in Italy*; Primicerio, M., Spigler, R., Valente, V., Eds.; World Scientific: Venice, 2004; p 1.

(19) Mahgerefteh, H.; Brown, S.; Martynov, S. A Study of the Effects of Friction, Heat Transfer, and Stream Impurities on the Decompression Behavior in CO_2 Pipelines. In *Greenhouse Gases: Science and Technology*; 2012; Vol. 2, p 369.

(20) Martynov, S.; Brown, S.; Mahgerefteh, H.; Sundara, V.; Chen, S.; Zhang, Y. Modelling Three-Phase Releases of Carbon Dioxide from High-Pressure Pipelines. *Process Saf. Environ. Prot.* **2014**, *92*, 36.

(21) Hammer, M.; Morin, A. A Method for Simulating Two-Phase Pipe Flow with Real Equations of State. *Comput. Fluids* **2014**, *100*, 45.

(22) Munkejord, S. T.; Hammer, M. Depressurization of CO_2-Rich Mixtures in Pipes: Two-Phase Flow Modelling and Comparison with Experiments. *Int. J. Greenh. Gas Control* **2015**, *37*, 398.

(23) Teng, L.; Li, Y.; Zhao, Q.; Wang, W.; Hu, Q.; Ye, X.; Zhang, D. Decompression Characteristics of CO_2 Pipelines Following Rupture. *J. Nat. Gas Sci. Eng.* **2016**, *36*, 213.

(24) Deligiannis, P.; Cleaver, J. W. Blowdown from a Vented Partially Full Vessel. *Int. J. Multiph. Flow* **1996**, *22*, 55.

(25) Bilicki, Z.; Kestin, J. Physical Aspects of the Relaxation Model in Two-Phase Flow. *Proc. R. Soc. A Math. Phys. Eng. Sci.* **1990**, *428*, 379.

(26) Brown, S.; Martynov, S.; Mahgerefteh, H.; Proust, C. A Homogeneous Relaxation Flow Model for the Full Bore Rupture of Dense Phase CO_2 Pipelines. *Int. J. Greenh. Gas Control* **2013**, *17*, 349.

(27) Lemmon, E. W.; Huber, M. L.; McLinden, M. O. NIST Standard ReferenceDatabase 23: Reference Fluid Thermodynamic and Transport Properties - REFPROP. NIST 2010.

(28) Soave, G. Equilibrium Constants from a Modified Redlich-Kwong Equation of State. *Chem. Eng. Sci.* **1972**, *27*, 1197.

(29) Peng, D. Y.; Robinson, D. B. A New Two-Constant Equation of State. *Ind. Eng. Chem. Fundam.* **1976**, *15*, 59.

(30) Valderrama, J. O. The State of the Cubic Equations of State. *Ind. Eng. Chem. Res.* **2003**, *42*, 1603.

(31) Kunz, O.; Wagner, W. The GERG-2008 Wide-Range Equation of State for Natural Gases and Other Mixtures: An Expansion of GERG-2004. *J. Chem. Eng. Data* **2012**, *57*, 3032.

(32) Gross, J.; Sadowski, G. Perturbed-Chain SAFT: An Equation of State Based on a Perturbation Theory for Chain Molecules. *Ind. Eng. Chem. Res.* **2001**, *40*, 1244.

(33) Mahgerefteh, H.; Wong, S. M. A. A Numerical Blowdown Simulation Incorporating Cubic Equations of State. *Comput. Chem. Eng.* **1999**, *23*, 1309.

(34) Overa, S. J.; Stange, E.; Salater, P. Determination of Temperature and Flare Rates during Depressurization and Fire. In *Proceedings of the annual convention - gas processors association*; San Antonio, 1994; p 235.

(35) Incropera, F. P.; De Witt, D. P. *Fundamentals of Heat and Mass Transfer*, 2nd ed.; John Wiley & Sons: New York, 1985.

(36) Liiey, P. E.; Thomson, G. H.; Friend, D. G.; Daubert, T. E.; Buck, E. Physical and Chemical Data. In *Perry's Chemical Engineers' Handbook*; Perry, R. H., Green, D. W., Maloney, J. O., Eds.; McGraw-Hill: New York, 2008; p 2.

(37) Powell, M. J. D. A Hybrid Method for Non-Linear Equations. In *Numerical methods for non-linear algebraic equations*; Rabinowitz, P., Ed.; Gordon and Breach Science Publishers: London, 1970.

(38) Blevins, R. D. *Applied Fluid Dynamics Handbook*; Van Nostrand Reinhold Company: New York, 1984.

(39) Moody, F. J. Maximum Flow Rate of a Single Component, Two-Phase Mixture. *J. Heat Transfer* **1965**, *87*, 134.

(40) Richardson, S.; Saville, G.; Fisher, S.; Meredith, A.; Dix, M. Experimental Determination of Two-Phase Flow Rates of Hydrocarbons through Restrictions. *Process Saf. Environ. Prot.* **2006**, *84*, 40.

(41) Ahmad, M.; Osch, M. B. Van; Buit, L.; Florisson, O.; Hulsbosch-Dam, C.; Spruijt, M.; Davolio, F. Study of the Thermohydraulics of CO_2 Discharge from a High Pressure Reservoir. *Int. J. Greenh. Gas Control* **2013**, *19*, 63.

(42) Woolley, R. M.; Fairweather, M.; Wareing, C. J.; Falle, S. A. E. G.; Mahgerefteh, H.; Martynov, S.; Brown, S.; Narasimhamurthy, V. D.; Storvik, I. E.; Sælen, L.; Skjold, L.; Economou, I. G.; Tsangaris, D. M.; Boulougouris, G. C.; Diamantonis, N.; Cusco, L.; Wardman, M.; Gant, S. E.; Wilday, J.; Zhang, Y. C.; Chen, S. Y.; Proust, C.; Hebrard, J.; Jamois, D. CO2PipeHaz: Quantitative Hazard Assessment for next Generation CO_2 Pipelines. In *Energy Procedia*; 2014; Vol. 63, p 2510.

(43) Mahgerefteh, H.; Brown, S.; Denton, G. Modelling the Impact of Stream Impurities on Ductile Fractures in CO_2 Pipelines. *Chem. Eng. Sci.* **2012**, *74*, 200.

LIST OF FIGURE CAPTIONS

Figure 1: A schematic representation of a pressure vessel during rapid depressurization showing the pertinent parameters for blowdown modeling.

Figure 2: The calculation flow diagram for determining the thermal states of the superheated liquid phase and the evaporated vapor.

Figure 3: Variation of the pressure with time for different discharge orifice diameters of 3 mm (a), 6 mm (b) and 12 mm (c).

Figure 4: Variations of liquid and the vapor zone temperatures with time for different discharge orifice diameters of 3 mm (a), 6 mm (b) and 12 mm (c).

Figure 5: Predicted decompression paths for TNO & DNV tests in pressure-temperature (p-T) plane.

Figure 6: Variation of pressure with time during INERIS test 2 (a), 9 (b) and 16 (c).

Figure 7: Variation of the liquid and vapor zone temperatures with time during INERIS test 2 (a), 9 (b) and 16 (c).

Figure 8: Measured and predicted pressure (a) and temperature (b) variations with time applying different constant relaxation times (from 0.005 to 0.5 s).

Figure 9: Predicted variation of the degrees of superheat of the liquid phase with time in the orifice diameter (a) and CO_2 purity (b) case studies.

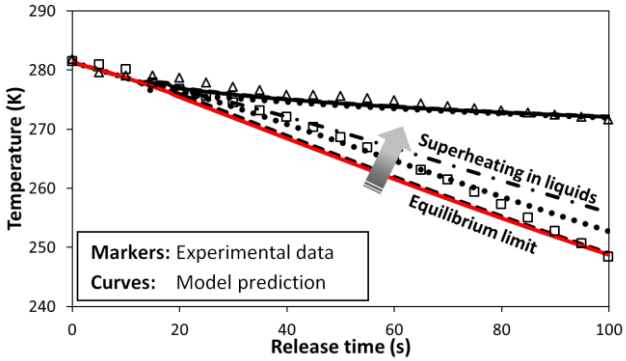

For Table of Contents Only.